Smart Structures and Systems, *Vol. 22, No. 4 (2018) 459-468*
DOI: https://doi.org/10.12989/sss.2018.22.4.459

Numerical simulation of shear mechanism of concrete specimens containing two coplanar flaws under biaxial loading

Vahab Sarfarazi[1], Hadi Haeri[*2] and Kourosh Bagheri[3]

[1]*Department of Mining Engineering, Hamedan University of Technology, Hamedan, Iran*
[2]*Young Researchers and Elite Club, Bafgh Branch, Islamic Azad University, Bafgh, Iran*
[3]*Department of civil engineering, Malard Branch, Islamic Azad University, Malard, Iran*

(Received July 1, 2018, Revised August 21, 2018, Accepted September 21, 2018)

Abstract. In this paper, the effect of non-persistent joints was determined on the behavior of concrete specimens subjected to biaxial loading through numerical modeling using particle flow code in two dimensions (PFC2D). Firstly, a numerical model was calibrated by uniaxial, Brazilian and triaxial experimental results to ensure the conformity of the simulated numerical model's response. Secondly, sixteen rectangular models with dimension of 100 mm by 100 mm were developed. Each model contains two non-persistent joints with lengths of 40 mm and 20 mm, respectively. The angularity of the larger joint changes from 30° to 90°. In each configuration, the small joint angularity changes from 0° to 90° in 30° increments. All of the models were under confining stress of 1 MPa. By using of the biaxial test configuration, the failure process was visually observed. Discrete element simulations demonstrated that macro shear fractures in models are because of microscopic tensile breakage of a large number of bonded discs. The failure pattern in Rock Bridge is mostly affected by joint overlapping whereas the biaxial strength is closely related to the failure pattern.

Keywords: rock bridge; non-persistent joint; PFC2D

1. Introduction

The propagation and coalescence of cracks originating from pre-existing joints in brittle materials such as rocks and concrete, through a variety of scales, are the dominant failure mechanisms that control the strength and integrity of the material. The presence of cracks controls the mechanical behaviour of rocks and concrete materials. Based on extensive research on cracking in brittle materials, such as rock and concrete, the two types of common cracks can be categorized as (a) tensile cracks (primary cracks) and (b) shear cracks (secondary cracks). The observed crack types have been the same in specimens with a single joint (flaw or discontinuity) or multiple joints. Tensile cracks initiate at the areas of tension at or near the tips of pre-existing joints and typically require an increase in the loading for an increase in propagation (Bobet and Einstein 1998, Bobet 2000). Crack coalescence, as the linkage of joints and flaws, occurs due to the initiation, propagation, and interaction of pre-existing and new cracks. Crack coalescence has been extensively studied in rock and concrete materials (e.g., Shen *et al.* 1995, Bobet and Einstein 1998, Sagong and Bobet 2002, Wong and Einstein 2007, 2009, Yaylac 2016, Wu *et al.* 2010, Lancaster *et al.* 2013, Ramadoss 2013, Pan *et al.* 2014, Mobasher *et al.* 2014, Noel and Soudki 2014, Haeri *et al.* 2014, Oliveira and Leonel 2014, Kim and Taha 2014, Tiang *et al.* 2015, Wan Ibrahim *et al*. 2015, Silva *et al.* 2015, Gerges *et al*. 2015, Liu e*t al.* 2015, Wasantha *et al.* 2015, Lee and Chang 2015, Kequan and Zhoudao 2015 Haeri *et al.* 2015a, b, Fan *et al.* 2016, Li *et al*. 2015, 2016, Sardemir 2016, Sarfarazi *et al*. 2016, Shuraim 2016, Akbas 2016, Rajabi 2016, Mohammad 2016, Shemirani *et al*. 2017, Wang *et al*. 2016, 2017). as well as in jointed materials (Haeri *et al.* 2016 a, b). The results from uniaxial compression experiments show that crack coalescence can be produced by the linkage of tensile cracks, shear cracks, or a combination of the two. Although many parameters, such as the quantity, geometry, and orientation of cracks, affect the coalescence patterns, the above three types of cracks are the most commonly observed. Due to the uncertainty and variety in the geometry, quantity, and orientation of cracks, the evaluation of cracking processes and the strength of materials is not feasible only through experiments. For this reason, a number of numerical techniques have been used to investigate the crack growth and coalescence. Discrete modeling techniques for fracturing processes in discontinuous rock masses and concrete have been widely reported. These originated as particle-based models (Cundall and Strack 1979, Zhang and Wong 2012, 2013, Sarfarazi *et al*. 2016a,b) or discrete element methods (DEM), which enable fracture modeling when combined with particle bonds that can break according to some loading criterion. These methods have evolved to provide related methods such as Discontinuous Deformation Analysis (DDA) and hybrid methods such as the finite-discrete element method (FDEM) (Munjiza *et al*. 1995) where features of both continuum and discrete modeling methodologies are combined (see e.g., Lisjak and Grasselli 2014 for a review of discrete modeling techniques).

In this paper, the particle flow code was used to study

*Corresponding author, Assistant Professor
E-mail: h.haeri@bafgh-iau.ac.ir

ISSN: 1738-1584 (Print), 1738-1991 (Online)

Table 1 micro properties used to represent the intact rock

Parameter	Value	Parameter	Value
Type of particle	disc	Parallel bond radius multiplier	1
Density (kg/m^3)	3500	Young modulus of parallel bond (GPa)	32
Minimum radius (mm)	0.27	Parallel bond stiffness ratio	2
Size ratio	1.56	Particle friction coefficient	0.5
Porosity ratio	0.08	Parallel bond normal strength, mean (MPa)	20
Damping coefficient	0.7	Parallel bond normal strength, SD (MPa)	2
Contact young modulus (GPa)	32	Parallel bond shear strength, mean (MPa)	20
Stiffness ratio	2	Parallel bond shear strength, SD (MPa)	2

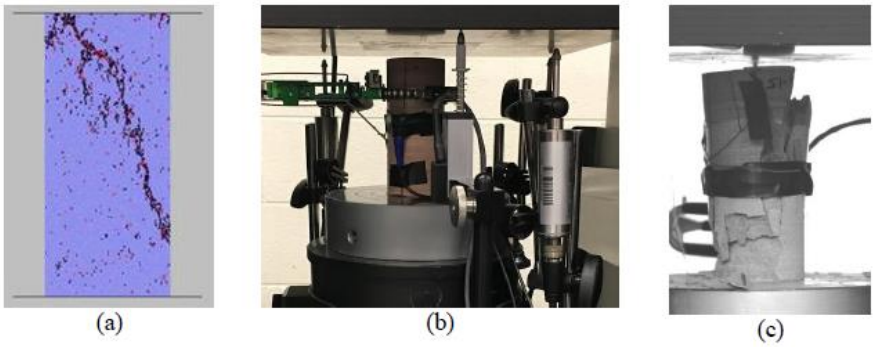

Fig. 1 (a) the failure pattern in numerical simulation, (b) experimental unconfined compressive test and (c) common failure mode of rock specimens

the failure behaviour of concrete samples consisting non-persistent joints under biaxial loading. For this purpose, by using an inverse-modelling calibration approach, the laboratory results of uniaxial, Brazilian and triaxial tests were examined to obtain the estimates of the intact concrete micromechanical parameters used in the simulation. The simulation was then performed to further evaluate the mechanical behaviour of the jointed models with different joint orientations. Calibration is done by done by trial and error.

2. Numerical modeling with PFC2D

Particle flow code represents a rock mass as an assemblage of bonded rigid particles (Cundall 1971, Potyondy and Cundall 2004). In its two dimensional version (PFC2D), circular disks are connected with cohesive and frictional bonds and confined with planar walls. Parallel bond model was adopted for this study to simulate the contacts between particles. Values assigned to the strength bonds influence the macro strength of sample and the nature of cracking and the failure occurs during the loading. Friction is activated by specifying coefficient of friction and is mobilized as long as the particles stay in contact. Tensile cracks occur when applied normal stress exceeds specified normal bond strength. Shear cracks are generated as applied shear stress surplus the specified shear bond strength either by rotation or by shearing of particles. Tensile strength at the contact immediately drops to zero after the bond breaks, while shear strength decreases to the residual friction value (Itasca Consulting Group Inc 2004, Cho *et al*. 2007, 2008, Potyondy and Cundall 2004). For all these microscopic behaviors, PFC requires only a selection of basic micro-parameters to describe contact, bond stiffness, bond strength and contact friction. But, these micro-parameters should provide a macro-scale behavior for the material being modeled. The code uses an explicit finite difference scheme to solve the equation of force and motion, and hence one can readily track the initiation and the propagation of bond breakage (fracture formation) through system (Potyondy and Cundall 2004). A calibrated PFC particle assembly was created by adopting the micro-properties listed in Table 1 and the standard calibration procedures (Potyondy and Cundall 2004).

2.1 Numerical unconfined compressive test

In PFC2D, the uniaxial compression test can be modelled by two moving walls compressing the particle assembly as illustrated in Fig. 1(a), with lines indicating the bonds breakages where the micro-cracks can be found. Black and red lines represent tensile and shear cracks, respectively. This failure pattern (Fig. 1(a)) is commonly observed in experiments. Walls were selected to be the frictionless rigid plates. This is like what happened in experimental test. Test specimens were 108 mm in height and 54 mm in width with the height to the width ratio of 2.

A normal particle size distribution was employed with particle radii of ranging from 0.27 to 0.4212 mm. The bounds of particles radii were chosen so to have particles as small as possible without compromising the computational efficiency and minimizing the code running time. Porosity value of 8% was selected for this packing. The modulus E,

(a) (b)

Fig. 2 The failure pattern in the (a) numerical model and (b) experimental samples

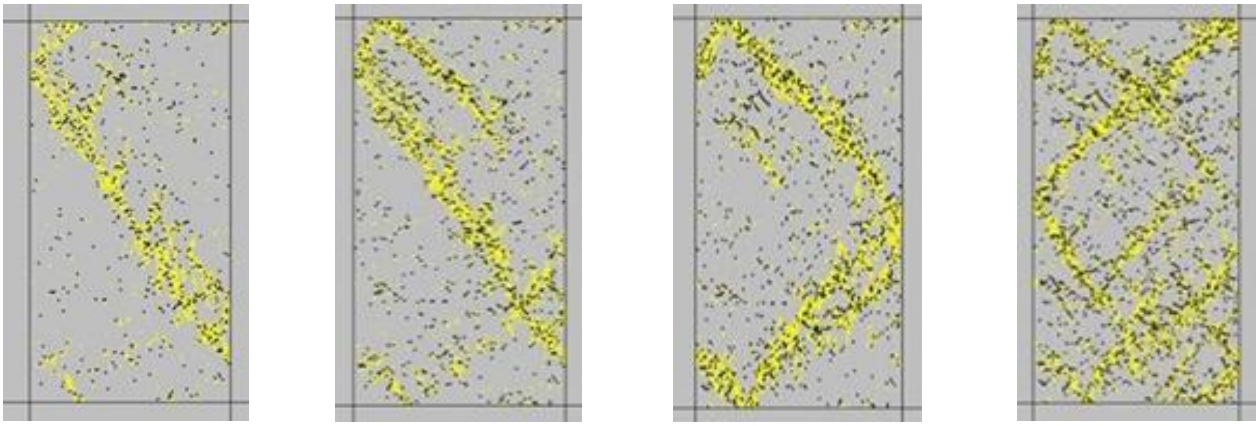

(a) (b) (c) (d)

Fig. 3 The fracture pattern in numerical models under confining pressure of (a) 0.5 MPa, (b) 1.5 MPa, (c) 2 MPa and (d) 3MPa

Poisson's ratio and uniaxial compression strength (UCS) of the particle assembly can be obtained through the PFC2D simulations. The procedure to determine these parameters were described by Itasca Consulting Group Inc., 2004.

Fig. 1(b) shows a conventional uniaxial compression specimen under loading. In the numerical model, an inclined fracture plane forms upon subsequent loading and as shown in Fig. 1(c), similar observation can be made from the experiments.

A comparison of numerical results with experimental data is presented in Table 2.

2.2 Brazilian test

The Brazilian test was used to calibrate tensile strength of specimen in the PFC2D models. Diameter of the Brazilian disk used in numerical tests was kept constant at 54 mm. The specimen was made of 5,615 particles. The disk was crushed by lateral walls, moving towards each other with a low speed of 0.016 m/s. Figs. 2(a) and 2(b) illustrate the failure patterns of numerical and experimental tested specimens, respectively. The failure patterns in numerical simulations and laboratory tests show a great agreement. Numerical tensile strength values are also compared with the experimental values in Table 2.

2.3 Biaxial test

Specifications for tested specimen in biaxial compression were similar to the unconfined compressive strength tests. For biaxial test, the rectangular model was loaded by the surrounding four walls.

The confining stress and the vertical stress were applied to the specimen by activating the servo-mechanism which controlled the velocities of the four confined walls. Fig. 3 shows the fracture patterns in numerical models under four different confining stresses.

Table 2 macro-mechanical properties of model material in experimental tests and PFC2D

Mechanical properties	Experimental results	PFC2D Model results
Elastic modulus (GPa)	33	33
Poisson's ratio	0.2	0.19
UCS (MPa)	18.3	18
Tensile strength (MPa)	2	4
Friction angle	28	23
Cohesion (MPa)	6	6.3

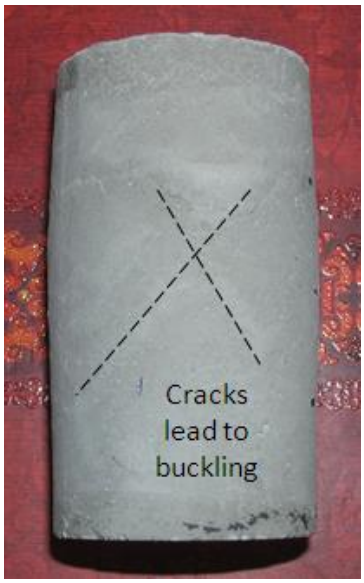

Fig. 4 the fracture pattern in numerical model under confining pressure of 3 MPa

When confining stress was 0.5 MPa (Fig. 3(a)), one major failure plane appeared in the specimen but for the confining stress of 3 MPa, several crossover failure planes appeared in the model (Fig. 3(d)). This failure pattern is quite similar to those occurring in tested specimens (Fig. 4). Cracks lead to buckling of the model.

It is to be not that the bonded-particle model (BPM) consisting of parallel-bonded disks or spheres suffers from the limitation that if one matches the unconfined-compressive strength of a typical hard concrete specimen, the direct-tension strength of the model will be too large (Potyondy and Cundall 2004). For concrete specimens, the tensile strength is about 1/10 of the compressive strength.

3.3 Numerical biaxial simulation of specimens with non-persistent open joints

3.3.1 Model development

After developing the calibrated models in PFC2D, several rectangular models were created to simulate the biaxial compression of concrete specimens containing non-persistent joints with different orientations and geometries (Figs. 5-8). The models were 100 mm by 100 mm and consisted of 21,179 disks with a minimum radius of 0.27 mm. Particles were surrounded by four walls. Non-persistent joints were formed by deletion of two bands of the particles from model, simulating the opening size (aperture) of 1 mm.

In total, sixteen specimens containing two non-persistent joints with different joint lengths and angles were set up to investigate the influence of ligament angle on failure behaviour of rock bridges. Each model contained two large and small non-persistent joints with lengths of 40 mm and 20 mm, respectively. The angularities of larger joint (α) changed from 30° (Fig. 5), 45° (Fig. 6), 60° (Fig. 7) and 90° (Fig. 8). In each configuration, the small joint angularities changed from 0° to 90° in 30° increments. The small joint was parallel to the large joint in first configuration and the orientation varied in the proceeding configurations until they became perpendicular (see Figs. 5(a)-5(d)). The joint spacing (i.e., the vertical distance between the inner tip of the small joint and the body of the larger joint) was 2 cm (Fig. 5(a)).

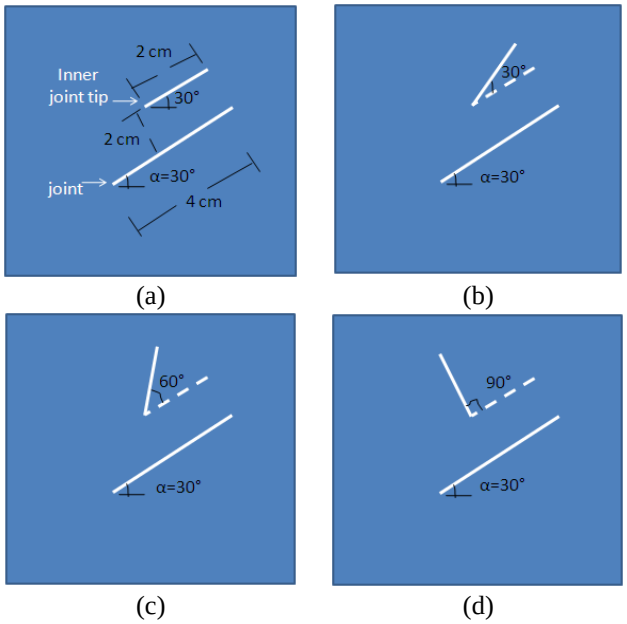

Fig. 5 Model with large joint angularity of 30 and small join angularity of; (a) 0°, (b) 30°, (c) 60° and (d) 90°

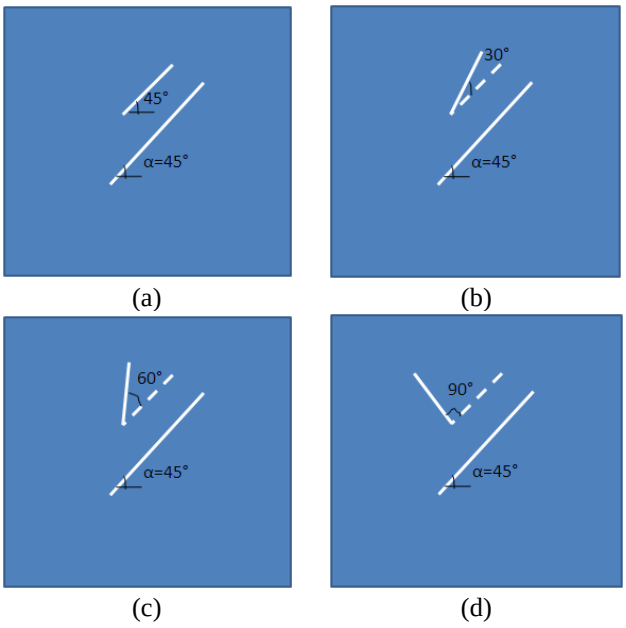

Fig. 6 Model with large joint angularity of 45 and small join angularity of; (a) 0°, (b) 30°, (c) 60° and (d) 90°

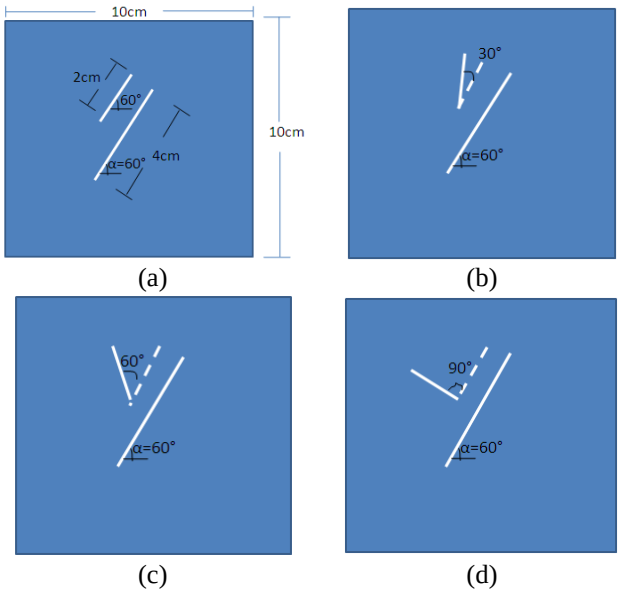

Fig. 7 Model with large joint angularity of 60 and small join angularity of; (a) 0°, (b) 30°, (c) 60° and (d) 90°

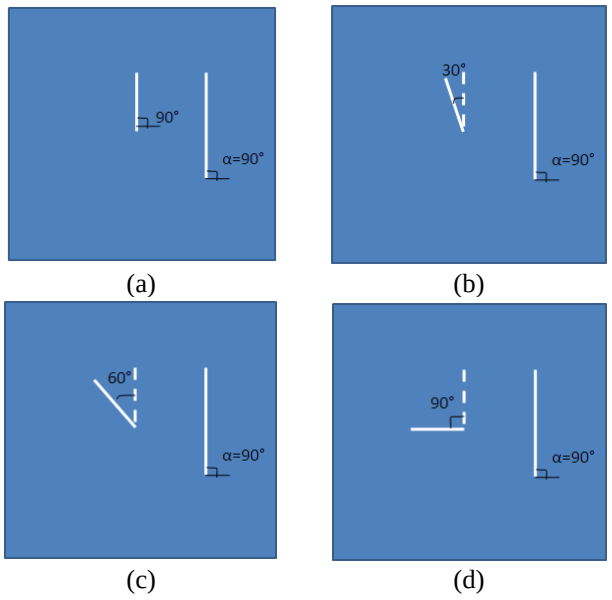

Fig. 8 Model with large joint angularity of 90 and small join angularity of; (a) 0°, (b) 30°, (c) 60° and (d) 90°

3.3.2 Load application

These models were loaded under the biaxial compression by firstly applying the confining (horizontal) stress and then applying the axial stress. With the existence of the non-persistent joints, such loading condition results in the development of tensile and shears cracks. Axial loading was applied to sample by moving the upper and lower walls in negative and positive Y-direction, respectively with a low velocity of 0.016 m/s to ensure a quasi-static equilibrium. The normal stress, 1 MPa, was kept constant by adjusting the right and left walls velocity using a numerical servo-mechanism. The axial displacements were measured by tracing the upper and lower wall displacements (Fig. 9). The axial stress was registered by taking the reaction forces on the lower wall in Fig. 9 and dividing the force by the cross section area.

4. Results and discussion

4.1 Effect of joint overlapping on failure behaviour of rock bridges

Figs. 10-13 illustrate the fracture patterns of non-persistent joints for α= 30°, 45°, 60° and 90°, respectively. The black and red lines represent the tensile and shear failures, respectively.

4.1.1 when α is 30°

When the large joint is oriented at 30° with respect to the horizontal axis, the tensile and shear cracks develop within the model for all of the configurations with different orientations of the smaller joint.

Configuration (a): When the small joint is parallel to the large joint, as seen in Fig. 10(a), the tensile cracks, indicated in black, initiate from the inner tip of the small joint and propagate diagonally till coalesce with the wall of the large joint. The cross set of shear bands develop within the model.

Configuration (b): When the small joint angle is 30° with respect to the orientation of the large joint, Fig. 10(b), the tensile cracks develop between outer tip of the small joint and the outer tips of the large joint. Also, a set of crossing shear bands develop within this model. There is no crack propagating from the inner tip of the small joint.

Configuration (c): When the small joint angle is 60° with respect to the orientation of the larger joint, Fig. 10(c), tensile cracks develop between the outer tip of the small join and the outer tips of the large joint. Also crossing shear cracks develop within the model.

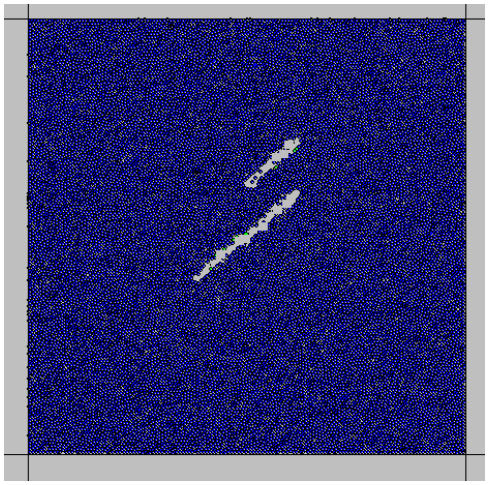

Fig. 9 Illustration of direct shear testing simulation scheme in PFC

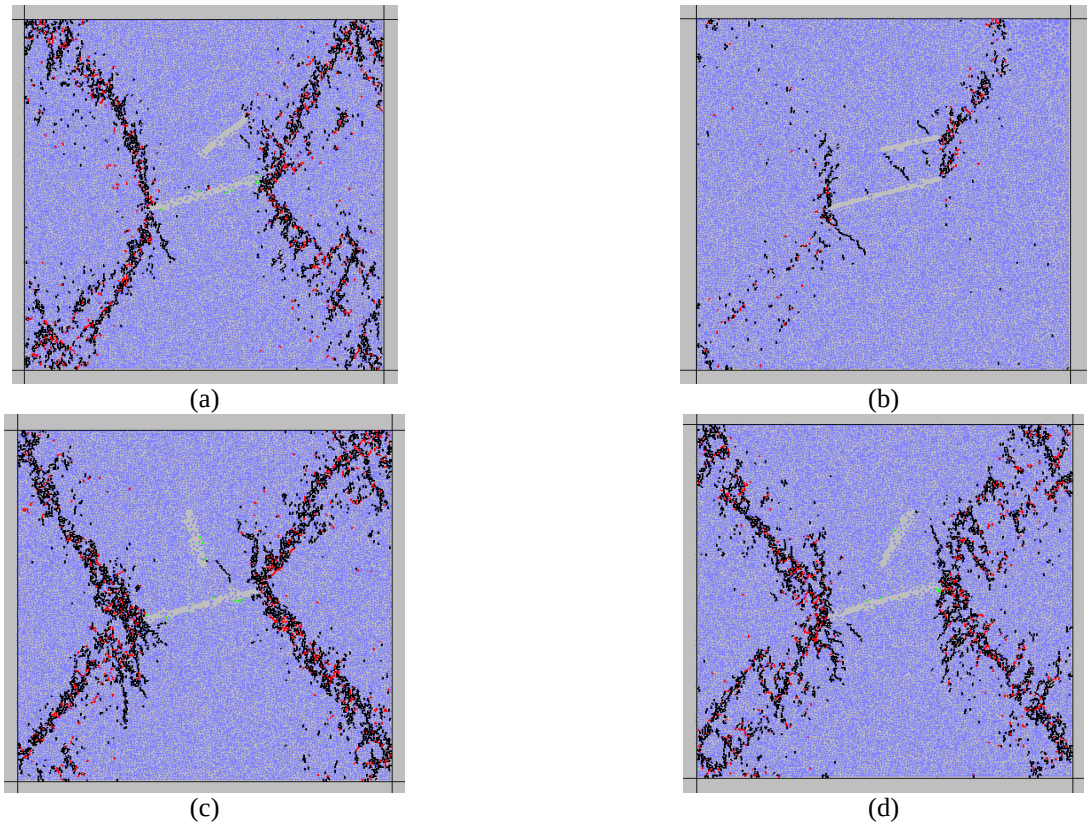

Fig. 10 Failure pattern in models with large joint angularity of 30 and small join angularity of; (a) 0°, (b) 30°, (c) 60° and (d) 90°

Configuration (d): When the small joint is perpendicular to the larger joint, Fig. 10d, the smaller joint has no influence on the mode of failure and the failure pattern consists of shear and tensile cracks forming from the tips of the large joint.

The significant difference between Fig. 10(a) and Figs. 10 (b)-10(d) is due to small joint angularity. The small joint angularities control the failure pattern. The bridge area between the small joint and large joint has drastic failure When small joint is nearly parallel to large joint direction.

4.1.2 when α is 45°

When the large joint angle is 45°, the tensile and shear cracks develop within the model for all of the small joint configurations (i.e., a-d).

Configuration (a): when the small joint is parallel to the large joint as seen in Fig. 11(a), cross set shear bands develop between the outer tip of the small joint and outer tip of the large joint. The cross set of shear bands develop within the model.

Configuration (b): when the small joint is oriented 30° with respect to the large joint, Fig. 11(b), cross set shear bands develop between the outer tip of small joint and outer tip of large joint. Also, the cross set of shear bands develop within the model. The inner tip of the smaller joint does not contribute to any cracking.

Configuration (c): For the small joint oriented 60° related to the large joint, Fig. 11(c), a cross set of shear bands develop within the model. There is no crack propagation from the smaller joint.

Configuration (d): With the small join perpendicular to the large joint, the model behaves as if the smaller joint does not exist and there is no major crack initiation from the tips or the walls of the smaller joint.

4.1.3 when α is 60°

When the large joint angle is 60°, the tensile and shear cracks develop within the model for all configurations of the smaller joint.

Configuration (a): As shown in Fig. 12(a), when the smaller joint is parallel to the larger joint, a set of shear bands develop within the model.

Configuration (b): When the small joint angle is 30° with respect to the large joint, Fig. 12(b), tensile cracks develop between inner tip of small join and outer tip of large joint. Also, a set of diagonal shear bands develop within the model.

Configuration (c): When the small joint angle is 60 with respect to the large joint, Fig. 12(c), the major cracks are the diagonal tensile and shear cracks originating from the tips of both small and large joints.

Configuration (d): For the smaller joint oriented perpendicular to the larger joint, Fig. 12(d), tensile cracks develop between inner tip of small joint and outer tip of the large joint.

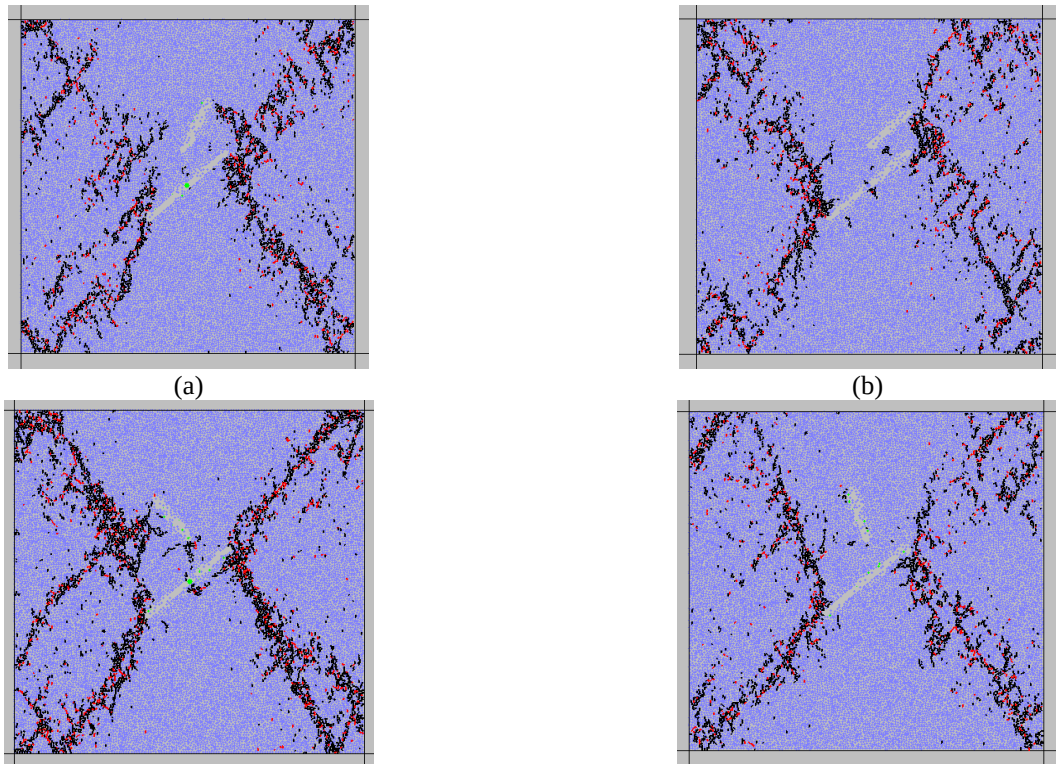

(a) (b) (c) (d)

Fig. 11 Failure pattern in models with large joint angularity of 45° and small join angularity of; (a) 0°, (b) 30°, (c) 60° and (d) 90°.

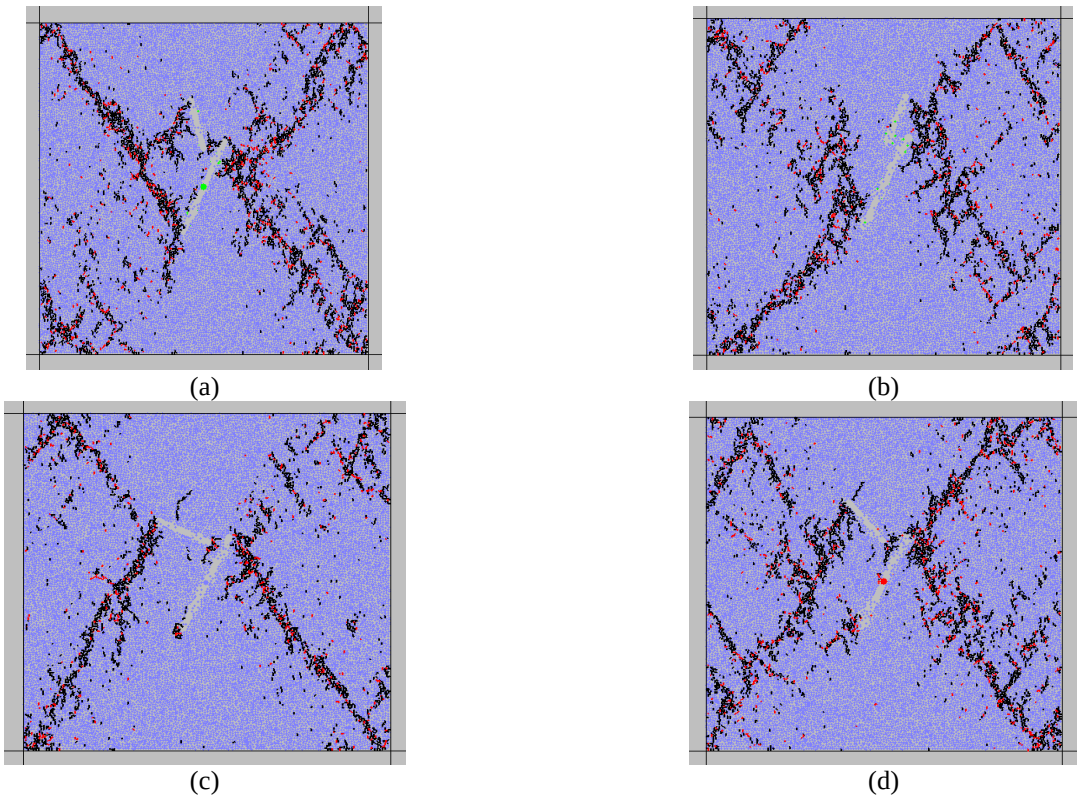

(a) (b) (c) (d)

Fig. 12 Failure pattern in models with large joint angularity of 60 and small join angularity of; (a) 0°, (b) 30°, (c) 60° and (d) 90°

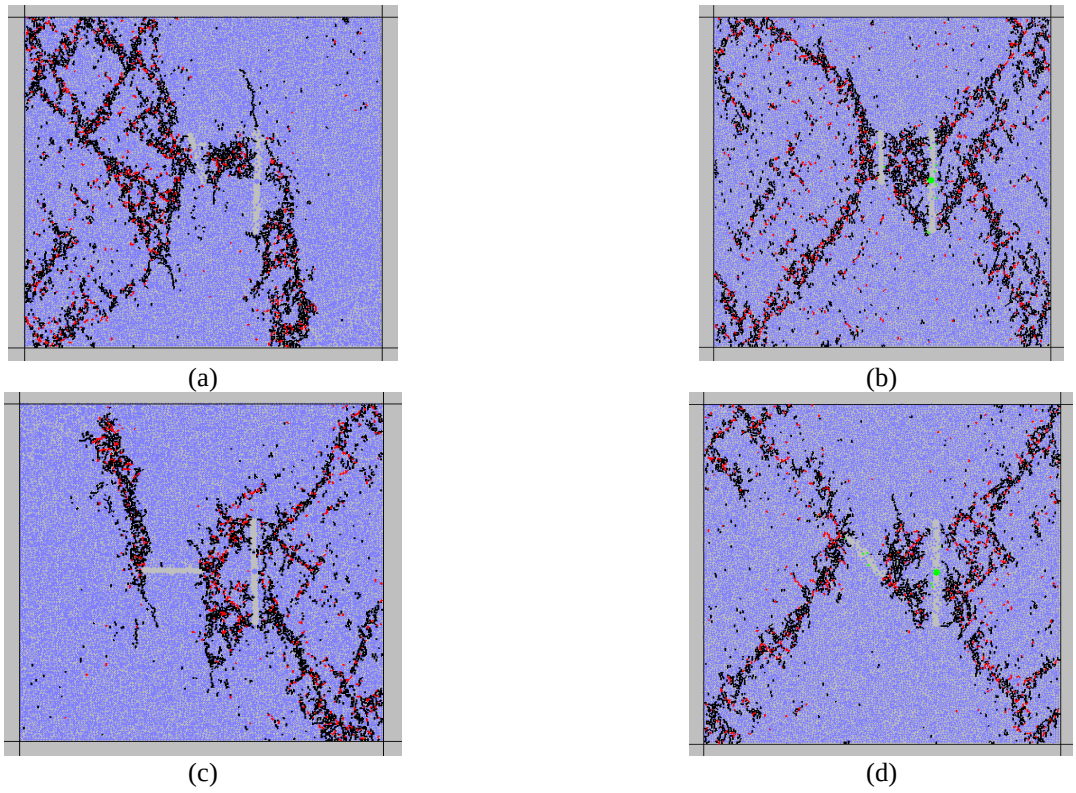

Fig. 13 Failure pattern in models with large joint angularity of 90° and small joint angularity of; (a) 0°, (b) 30°, (c) 60° and (d) 90°

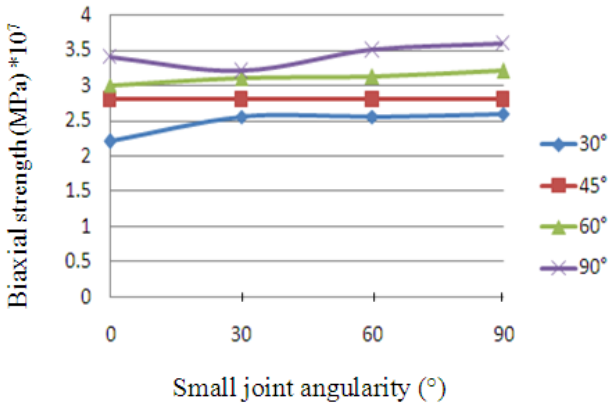

Fig. 14 shows variation of biaxial strength versus the small joint angularity for four different large joint angularities

4.1.4 when α is 90°

When the large joint angle is 90°, the tensile and shear cracks develop within the model for four small joint configurations (Fig. 13). For all of these configurations, a set of shear bands develop between the small joint and large joint.

For all configurations as seen in Fig. 13, cross set shear bands develop between the small joint and large joint. Also, the cross set of shear bands develop within the model.

4.4.2 The effect of small joint angularity on the biaxial strength

Fig. 14 shows variation in the biaxial strength values as a function of small joint angularity for four different large joint angularities, i.e., 30°, 45°, 60° and 90°. The biaxial strength increases with increasing the both of the large joint angularities and small joint angularities. The impact of the small joint angularity seems to be limited.

5. Conclusions

Biaxial behavior of concrete specimens containing two joints with different overlapping was investigated by means of numerical simulations. The following conclusions can be drawn from this research:

- Numerical experiments reported in this paper showed that the both of the tension and shear cracks are responsible for failure of the model.
- Failure pattern is highly dependent on joint overlapping. The rock bridges are broken with the increase in the large joint angularity. The rock bridge damage increases as the small joint angularity increases.
- Shear band occurrence increases in models with increasing the large joint angularity. The impact of the small joint angularity seems to be limited.
- When the large joint is oriented at 30° with respect to the horizontal axis and small joint is parallel to the large joint, the tensile cracks initiate from the inner tip of the small joint and propagate diagonally till coalesce with the wall of the large joint. The cross set of shear bands develop within the model. When the small joint angle is 30° with respect to the orientation of the large joint, the tensile cracks develop between outer tip of the small joint and the outer tips of the large joint. Also, a set of crossing shear bands develop within this model. There is no crack propagating from the inner tip of the small joint. When the small joint angle is 60° with respect to the orientation of the larger joint, tensile cracks develop between the outer tip of the small join and the outer tips of the large joint. Also crossing shear cracks develop within the model. When the small joint is perpendicular to the larger joint, the smaller joint has no influence on the mode of failure and the failure pattern consists of shear and tensile cracks forming from the tips of the large joint.
- When the large joint angle is 45° and the small joint is parallel to the large joint, cross set shear bands develop between the outer tip of the small joint and outer tip of the large joint. The cross set of shear bands develop within the model. When the small joint is oriented 30° with respect to the large joint, cross set shear bands develop between the outer tip of small joint and outer tip of large joint. Also, the cross set of shear bands develop within the model. The inner tip of the smaller joint does not contribute to any cracking. For the small joint oriented 60° related to the large joint, a cross set of shear bands develop within the model. There is no crack propagation from the smaller joint. With the small joint perpendicular to the large joint, the model behaves as if the smaller joint does not exist and there is no major crack initiation from the tips or the walls of the smaller joint.
- When the large joint angle is 60° and the smaller joint is parallel to the larger joint, a set of shear bands develop within the model. When the small joint angle is 30° with respect to the large joint, tensile cracks develop between inner tip of small join and outer tip of large joint. Also, a set of diagonal shear bands develop within the model. When the small joint angle is 60 with respect to the large joint, the major cracks are the diagonal tensile and shear cracks originating from the tips of both small and large joints. For the smaller joint oriented perpendicular to the larger joint, tensile cracks develop between inner tip of small joint and outer tip of the large joint.
- When the large joint angle is 90°, the tensile and shear cracks develop within the model for four small joint configurations. For all of these configurations, a set of shear bands develop between the small joint and large joint.

References

Akbas, S. (2016), "Analytical solutions for static bending of edge cracked micro beams", *Struct. Eng. Mech.*, **59**(3), 66-78.

Bobet, A. (2000), "The initiation of secondary cracks in compression", *Eng. Fract. Mech*., **66**, 187-219.

Bobet, A. and Einstein, H.H. (1998), "Fracture coalescence in rock-type materials under uniaxial and biaxial compression", *Int. J. Rock Mech. Min. Sci*., **35**, 863-888.

Cundall, P.A. and Strack, O.D.L. (1979), "A discrete numerical model for granular assemblies", *Geotechnique*, **29**(1), 47-65.

Fan, Y., Zhu, Z., Kang, J. and Fu, Y. (2016), "The mutual effects between two unequal collinear cracks under compression", *Math. and Mech.Solids*, **22**,1205-1218.

Gerges, N., Issa, C. and Fawaz, S. (2015), "Effect of construction joints on the splitting tensile strength of concrete", *Case Studies in Construction Materials*, **3**, 83-91.

Haeri, H., Khaloo, A. and Marji, M.F. (2015a), "Fracture analyses of different pre-holed concrete specimens under compression", *Acta mechanica sinica*, **31**(6), 855-870.

Haeri, H., Khaloo, A. and Marji, M.F. (2015b), "A coupled experimental and numerical simulation of rock slope joints behavior" , *Arabian J. Geosci*., **8**(9), 7297-7308.

Haeri, H., Sarfarazi, V. and Lazemi, H.A. (2016b), "Experimental study of shear behavior of planar non-persistent joint", *Comput. Concrete*, **17**(5), 639-653.

Haeri, H., Sarfarazi, V., Fatehi, M., Hedayat, A. and Zhu, Z. (2016a), "Experimental and numerical study of shear fracture in brittle materials with interference of initial double", *Acta Mechanica Soilda sinica*, **5**, 555-566.

Haeri, H., Shahriar, K., Fatehi Marji, M. and Moarefvand, P. (2014), "On the crack propagation analysis of rock like Brazilian disc specimens containing cracks under compressive line loading", *Latin Am. J. Solids Struct*., **11**(8), 1400-1416.

Ibrahim, M.H.W, Hamzah, A.F., Jamaluddin, N., Ramadhansyah, P.J. and Fadzil, A.M. (2015), "Split tensile strength on self-compacting concrete containing coal bottom ash", *Procedia - Social Behavioral Sci.*, **198**, 2280-2289.

Kequan, Y.U. and Zhoudao, L.U, (2015), "Influence of softening curves on the residual fracture toughness of post-fire normal-strength mortar", *Comput. Mortar*, **15**(2), 102-111.

Lancaster, I.M., Khalid, H.A. and Kougioumtzoglou, I.A. (2013), "Extended FEM modelling of crack propagation using the semi-circular bending test", *Constr. Build. Mater*., **48**, 270-277.

Lee, S. and Chang, Y. (2015), "Evaluation of RPV according to alternative fracture toughness requirements", *Struct. Eng. Mech*., **53**(6), 1271-1286.

Li, S., Wang, H., Li, Y., Li, Q., Zhang, B. and Zhu, H. (2016), "A new mini-grating absolute displacement measuring system for static and dynamic geomechanical model tests", *Measurement*, **82**, 421-431.

Li, S., Wang, H., Li, Y., Li, Q., Zhang, B. and Zhu, H. (2016), "A new mini-grating absolute displacement measuring system for

static and dynamic geomechanical model tests", *Measurement*, **82**, 421-431.

Li, Y., Zhou, H., Zhu, W., Li, S. and Liu, J. (2015), "Numerical study on crack propagation in brittle jointed rock mass influenced by fracture water pressure", *Materials*, **8**(6), 3364-3376.

Lisjak, A. and Grasselli, G. (2014), "A review of discrete modeling techniques for fracturing processes in discontinuous rock masses", *J. Rock Mech. Geotech. Eng*., **6**(4), 301-314.

Liu, X., Nie, Z., Wu, S. and Wang, C, (2015), "Self-monitoring application of conductive asphalt concrete under indirect tensile deformation", *Case Studies Constr. Mater*., **3**, 70-77.

Lu, F.Y., Lin, Y.L., Wang, X.Y., Lu, L. and Chen, R. (2015), "A theoretical analysis about the influence of interfacial friction in SHPB tests", *Int. J. Impact. Eng*., **79**, 95-101.

Mobasher, B., Bakhshi, M. and Barsby, C. (2014), "Backcalculation of residual tensile strength of regular and high performance fibre reinforced concrete from flexural tests", *Constr. Build. Mater.*, **70**, 243-253.

Mohammad, A. (2016), "Statistical flexural toughness modeling of ultra-high performance mortar using response surface method", *Comput. Mortar* , **17**(4), 33-39.

Munjiza, A., Owen, D.R.J. and Bicanic, N.A. (1995), "A combined finite-discrete element method in transient dynamics of fracturing solids", *Eng. Comput*., **12**(2), 145-174.

Noel, M. and Soudki, K. (2014), "Estimation of the crack width and deformation of FRP-reinforced concrete flexural members with and without transverse shear reinforcement", *Eng. Struct*., **59**, 393-398.

Oliveira, H.L. and Leonel, E.D. (2014), "An alternative BEM formulation, based on dipoles of stresses and tangent operator technique, applied to cohesive crack growth modeling", *Eng. Anal. Bound. Elem*., **41**, 74-82.

Pan, B., Gao, Y. and Zhong, Y. (2014), "Theoretical analysis of overlay resisting crack propagation in old cement mortar pavement", *Struct. Eng. Mech*., **52**(4), 167-181.

Rajabi, M., Soltani, N. and Eshraghi, I. (2016), "Effects of temperature dependent material properties on mixed mode crack tip parameters of functionally graded materials", *Struct. Eng. Mech*., **58**(2), 144-156.

Ramadoss, P. and Nagamani, K. (2013), "Stress-strain behavior and toughness of high-performance steel fiber reinforced mortar in compression", *Comput. Mortar*, **11**(2), 55-65.

Sagong, M. and Bobet, A. (2002), "Coalescence of multiple flaws in a rock-model material in uniaxial compression", *Int. J. Rock. Mech. Min*., 399-241.

Sardemir, M. (2016), "Empirical modeling of flexural and splitting tensile strengths of concrete containing fly ash by GEP", *Comput. Concrete*, **17**(4), 489-498.

Sarfarazi, V. and Shubert, W. (2016b), "Sliding phenomena in intermittent rock joint", *Periodica polyechnica civil engineering*, **5**, 1-10.

Sarfarazi, V., Haeri, H. and khaloo, A (2016a), "The effect of non-persistent joints on sliding direction if rock slopes", *Comput. Concrete*, **7**, 723-737.

Shemirani, A., Haeri, H., Sarfarazi, V. and Hedayat, A. (2017), "A review paper about experimental investigations on failure behavior of non-persistent joint", *Geomech. Eng*., **13**, 535-570.

Shen, B., Stephansson, O., Einstein, H.H. and Ghahreman, B. (1995), "Coalescence of fractures under shear stress experiments", *J. Geophys.Res.*, **100**(4), 5975-5990.

Shuraim, A.B., Aslam, F., Hussain, R. and Alhozaimy, A. (2016), "Analysis of punching shear in high strength RC panels–experiments, comparison with codes and FEM results", *Comput. Concrete*, **17**(6), 739-760.

Silva, R.V., Brito, J. and Dhir, R.K. (2015), "Tensil strength behaviour of recycled aggregate concrete", *Constr. Build. Mater*., **83**, 108-118.

Tiang, Y., Shi, S., Jia, K. and Hu, S. (2015), "Mechanical and dynamic properties of high strength concrete modified with lightweight aggregates presaturated polymer emulsion", *Constr. Build. Mater*., **93**, 1151-1156.

Wang, Q.Z., Feng, F., Ni, M. and Gou, X.P. (2011), "Measurement of mode I and mode II rock dynamic fracture toughness with cracked straight through flattened Brazilian disc impacted by split Hopkinson pressure bar", *Eng. Fract. Mech*., **78**(12), 2455-2469

Wang, X., Zhu, Z., Wang, M., Ying, P., Zhou, L. and Dong, Y. (2017), "Study of rock dynamic fracture toughness by using VB-SCSC specimens under medium-low speed impacts", *Eng. Fract. Mech*., **181**, 52-64.

Wong, L.N.Y. and Einstein, H.H. (2008), "Systematic evaluation of cracking behavior in specimens containing single flaws under uniaxial compression", I*nt. J. Rock Mech. Min*., **46**(2), 239-249.

Wong, L.N.Y. and Einstein, H.H. (2009), "Crack coalescence in molded gypsum and Carrara marble: part 2- microscopic observations and interpretation", *Rock Mech. Rock Eng*., **42**(3), 513-545.

Wu, Z.J., Ngai, L. and Wong, Y. (2014), "Investigating the effects of micro-defects on the dynamic properties of rock using Numerical Manifold method", *Constr. Build Mater*., **72**, 72-82.

Yaylac, M. (2016), "The investigation crack problem through numerical analysis", *Struct. Eng. Mech*., **57**(6), 1143-1156.

Zhang, Q.B. and Zhao, J (2014), "Quasi-static and dynamic fracture behaviour of rock materials: phenomena and mechanisms", *Int. J. Fract*., **189**, 1-32

Zhang, X.P. and Wong, L.N.Y. (2012), "Cracking process in rock-like material containing a single flaw under uniaxial compression: A numerical study based on parallel bonded-particle model approach", *Rock Mech. Rock Eng*., **45**(5), 711-737.

Zhang, X.P. and Wong, R.H.C. (2013), "Crack initiation, propagation and coalescence in rock-like material containing two flaws: A numerical study based on bonded-particle model approach", *Rock Mech. Rock Eng*., **46**(5), 1001-1021.

Zhao, Y., Zhao, G.F. and Jiang, Y. (2013), "Experimental and numerical modelling investigation on fracturing in coal under impact loads", *Int. J. Fract*, **183**(1), 63-80.

CC